Article

# Characterization of Structurally Diverse $^{18}$F-Labeled d-TCO Derivatives as a PET Probe for Bioorthogonal Pretargeted Imaging

Karuna Adhikari, Jonatan Dewulf, Christel Vangestel, Pieter Van der Veken, Sigrid Stroobants, Filipe Elvas,* and Koen Augustyns*

Read Online

ACCESS | Metrics & More | Article Recommendations | Supporting Information

**ABSTRACT:** *Background*: The pretargeted imaging strategy using inverse electron demand Diels−Alder (IEDDA) cycloaddition between a *trans*-cyclo-octene (TCO) and tetrazine (Tz) has emerged and rapidly grown as a promising concept to improve radionuclide imaging and therapy in oncology. This strategy has mostly relied on the use of radiolabeled Tz together with TCO-modified targeting vectors leading to a rapid growth of the number of available radiolabeled tetrazines, while only a few radiolabeled TCOs are currently reported. Here, we aim to develop novel and structurally diverse $^{18}$F-labeled cis-dioxolane-fused TCO (d-TCO) derivatives to further expand the bioorthogonal toolbox for *in vivo* ligation and evaluate their potential for positron emission tomography (PET) pretargeted imaging. *Results*: A small series of d-TCO derivatives were synthesized and tested for their reactivity against tetrazines, with all compounds showing fast reaction kinetics with tetrazines. A fluorescence-based pretargeted blocking study was developed to investigate the *in vivo* ligation of these compounds without labor-intensive prior radiochemical development. Two compounds showed excellent *in vivo* ligation results with blocking efficiencies of 95 and 97%. Two novel $^{18}$F-labeled d-TCO radiotracers were developed, from which [$^{18}$F]MICA-214 showed good *in vitro* stability, favorable pharmacokinetics, and moderate *in vivo* stability. Micro-PET pretargeted imaging with [$^{18}$F]MICA-214 in mice bearing LS174T tumors treated with tetrazine-modified CC49 monoclonal antibody (mAb) (CC49-Tz) showed significantly higher uptake in tumor tissue in the pretargeted group (CC49-Tz 2.16 ± 0.08% ID/mL) when compared to the control group with nonmodified mAb (CC49 1.34 ± 0.07% ID/mL). *Conclusions*: A diverse series of fast-reacting fluorinated d-TCOs were synthesized. A pretargeted blocking approach in tumor-bearing mice allowed the choice of a lead compound with fast reaction kinetics with Tz. A novel $^{18}$F-labeled d-TCO tracer was developed and used in a pretargeted PET imaging approach, allowing specific tumor visualization in a mouse model of colorectal cancer. Although further optimization of the radiotracer is needed to enhance the tumor-to-background ratios for pretargeted imaging, we anticipate that the $^{18}$F-labeled d-TCO will find use in studies where increased hydrophilicity and fast bioconjugation are required.
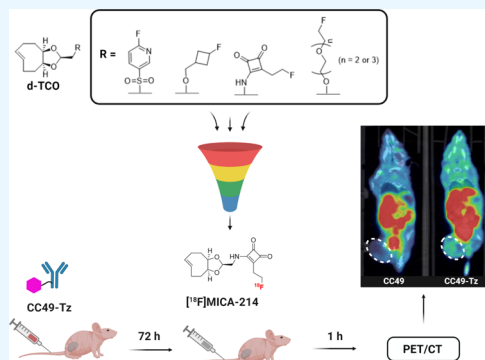
## INTRODUCTION

Bioorthogonal chemistry for pretargeted imaging through inverse electron demand Diels−Alder (IEDDA) reaction between a 1,2,4,5-tetrazine (Tz) and a *trans*-cyclooctene (TCO) with its ultrafast kinetics and selectivity has attracted considerable interest in the field of targeted delivery of radionuclides and molecular imaging.[1−3] Immuno-positron emission tomography (Immuno-PET) is an imaging technique that combines the selectivity and affinity of monoclonal antibodies (mAbs) with the high resolution and sensitivity of PET to visualize and quantify specific biomolecules or cells *in vivo*.[4] However, the slow pharmacokinetics of antibodies requires the use of long-lived radioisotopes leading to high radiation exposure in nontarget organs. A pretargeted immuno-PET imaging through an IEDDA reaction between a TCO and Tz uses the specificity of antigen-mAb interaction and has the advantage of enabling the use of short-lived radioisotopes in a

multistep approach.[5] Briefly, an antibody is injected first and accumulates in the target before a small radiolabeled molecule is administered after a few days of clearance of the long-circulating antibody. These two moieties react *in vivo* through biorthogonal chemistry. The unbound fraction of the radio-labeled molecule is then rapidly excreted from circulation.[6] The temporal separation of the antibody from the radioactivity administration allows the use of short-lived radioisotopes such as fluorine-18 [$^{18}$F]F$^-$ ($t_{1/2}$ = 110 min) with favorable decay properties (97% $\beta^+$ emission, 634 keV maximum $\beta^+$ energy)
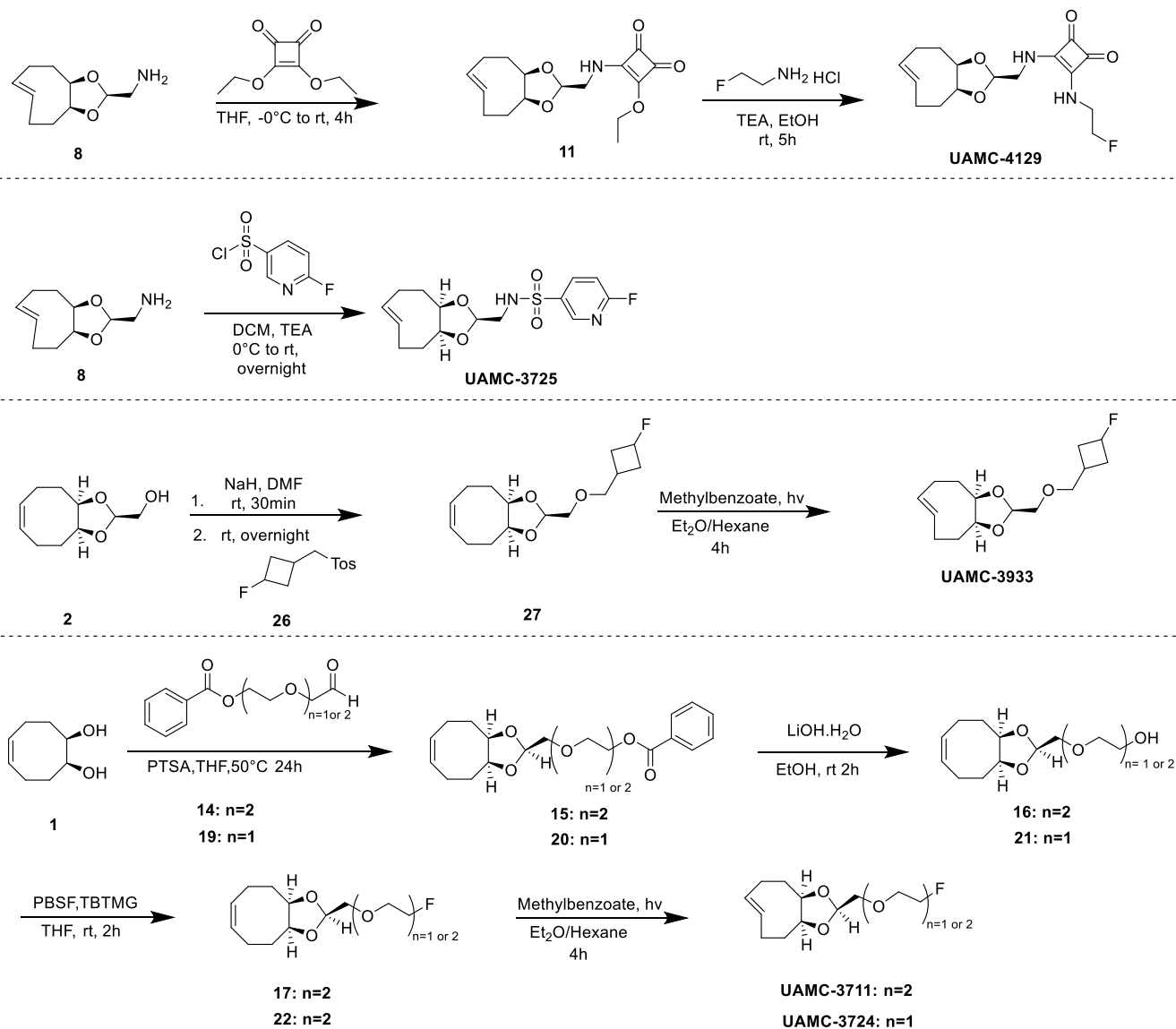
## Scheme 1. Synthesis of d-TCO Derivatives



and short $\beta^+$ trajectory in tissues (<2.3 mm) for high-resolution PET imaging.[7] The use of short-lived isotopes also leads to lower radiation burden to the patient during the imaging and improved tumor-to-background ratios resulting in high-contrast PET images.

Considerable research has been devoted to the pretargeted imaging approach with $[^{18}F]F^-$ using biorthogonal chemistry where TCO-Tz ligation has become the gold standard.[5,8] Apart from its selectivity and biorthogonality, TCO-Tz ligation shows ultrafast kinetics with the first-order rate constant up to $10^{6-7}$ $M^{-1}$ $s^{-1}$. The exceptionally fast reaction kinetics plays a pivotal role in the feasibility of *in vivo* pretargeted imaging.[9] With the advances in the field of bioorthogonal chemistry and tetrazine labeling, numerous studies have been reported where the ligation between a mAb conjugated to TCO and $^{18}F$-radiolabeled-Tz pair was used for pretargeted tumor imaging.[10−14] Although lower absolute tumor uptake values were observed, improved tumor-to-background ratios have been obtained using $^{18}F$-labeled Tz when compared to the "state-of-the-art" chelator-based radiolabeled tetrazines.[15,16] In principle, both tetrazines and TCO can be radiolabeled.

However, the inverse approach, where the TCO is radiolabeled and the tetrazine is conjugated to mAb, is still less explored. Nevertheless, it has been shown that TCO directly conjugated to mAb tends to bury within the protein core, leaving only a few reactive tags available. This could be circumvented by extending the distance between the targeting and the reactive moiety, by introducing, for example, hydrophilic PEG linkers.[17] Moreover, TCO also isomerizes to its less reactive cis-form in circulation.[18] Furthermore, the polarity of radiolabeled tetrazines restricts the imaging of noninternalizing and peripheral targets. Thus, the replacement of the TCO tags with tetrazines could offer an alternative to circumvent the prolonged exposure of TCO to physiological conditions and enable the visualization of internalizing targets, owing to the increased cell permeability of TCOs. $[^{18}F]FTCO$, initially developed as an $^{18}F$-labeling strategy for preassembled $[^{18}F]FTCO$-Tz targeting molecules, showed poor metabolic stability *in vivo* for pretargeted imaging.[19,20] Later, a more stable TCO-NOTA derivative was successfully radiolabeled through chelation with $Al[^{18}F]F$ and used to visualize LS174T tumor xenografts.[21] In recent years, new generations of faster

and more stable conformationally strained cyclopropane-fused TCO (sTCO) and cis-dioxolane-fused TCO (d-TCO) have been described. These are often employed to track and image fast biological processes and as labeling agents for the assembly of PET probes.[9,22−24] The use of d-TCOs may improve the *in vivo* ligation due to their improved kinetics, stability, and increased aqueous solubility. However, only a few ^{18}F-labeled d-TCO's have been used for pretargeting applications. In 2017, Billaud et al. reported on the initial use of an ^{18}F-labeled d-TCO probe in a pretargeted imaging setting. The tracer showed favorable *in vitro* stability and pharmacokinetics, while the absolute tumor uptake in the pretargeted approach remained low with substantial abdominal background activity.[25] In 2020, a new d-TCO amide derivative was successfully used by our group in a pretargeting study in LS174T tumor-bearing mice.[26] Despite improved tumor uptake values being achieved, the tumor-to-background ratio could yet be optimized. These findings highlight the need for the development of more diverse and improved TCO structures with improved stability, reactivity, and pharmacokinetic profile, which are critical for understanding the role of different variables in pretargeted imaging via bioorthogonal TCO-Tz ligation and steering its future as a powerful diagnostic tool.

Here, we report the synthesis of a small series of fluorinated d-TCO derivatives and the initial screening of their *in vivo* reactivity through a pretargeted blocking study. The d-TCO core was modified with sulfonyl fluoropyridine, short poly-(ethylene glycol) (PEG) chains, a cyclobutyl ring, and squaramide as linkers. These linkers were chosen to modulate the lipophilicity of the d-TCO core to minimize the nonspecific tracer accumulation while also impacting the overall metabolic stability of the radiotracer *in vivo*.[27−30] The probe that yielded the highest blocking signal was selected for further radiochemical development and pharmacokinetics studies. Finally, a pretargeted μPET imaging experiment was performed in mice bearing LS174T human colorectal tumors pretreated with a tetrazine-modified anti-TAG-72 monoclonal antibody (CC49) to visualize the tumor.

## RESULTS

**Synthesis of d-TCO Derivatives.** Five d-TCOs with structurally diverse linkers were synthesized. The d-TCO-amide derivatives were synthesized from the d-TCO-amine scaffold, as previously described.[26] **UAMC-4129** was synthesized in two steps by reacting the d-TCO-amine with diethyl squarate followed by nucleophilic substitution with a 2-fluoroethylamine (Scheme 1). Similarly, the nucleophilic substitution of 6-fluoropyridine-3-sulfonyl chloride with the d-TCO-amine afforded sulfonamide **UAMC-3725** (Scheme 1). Compound **2** (syn diastereomer) was obtained following a previously reported procedure.[9] In parallel, the cyclobutyl intermediate **26** was prepared in four steps starting from the reduction of 3-(benzyloxy)cyclobutane-1-carboxylic acid. The obtained alcohol was tosylated, followed by the removal of the benzyl-protecting group through hydrogenation on Pd/C. The alcohol was fluorinated with perfluoro-1-butanesulfonyl fluoride (PBSF) to afford **26**. Compound **2** was deprotonated with sodium hydride followed by nucleophilic substitution of the tosyl group on **26** to afford **27**, which was finally photoisomerized in a closed-loop flow photoreactor to afford the desired reference compound **UAMC-3933** (Scheme 1). The synthesis of **UAMC-3711** and **UAMC-3724** was carried

out through modification of a reported procedure.[22] Starting from diethylene or triethylene glycol, PEG synthons **14** and **19** were prepared in two steps by first protecting one of the hydroxyl groups with benzoyl chloride (BzCl). In the second step, the other hydroxyl was oxidized to an aldehyde in the presence of the Dess−Martin periodinane reagent. In parallel, the oxidation of 1,5-cyclooctadiene into diol **1** was carried out using OsO₄. Diol **1** was acetalized with **14** or **19** affording the dioxolane **15** and **20**, respectively, with syn diastereomer as the major product. After deprotection using LiOH, the hydroxyl group was fluorinated with PBSF to afford **17** or **22**, and finally, the *trans-for-cis* photoisomerization gave the references **UAMC-3711** and **UAMC-3724** (Scheme 1).

**Reaction Kinetics of d-TCOs with Tetrazine.** Second-order rate constants for the reaction of the synthesized d-TCOs with tetrazines were determined by pseudo-first-order measurements in a stopped-flow photometer at 37 °C in a solvent system consisting of MeOH/H₂O 50:50 (v/v). With 6-methylbenzylamine tetrazine (MeBA), the rate constants measured were in the range 2067−4802 M⁻¹ s⁻¹ (Table 1;

**Table 1. Calculated log *D* and Rate Constants of Synthesized d-TCOs with MeBA and 2Pyr₂ in MeOH/H₂O at 37 °C**

| TCO | log $D$ | $k_2$ (M⁻¹ s⁻¹) MeBA | $k_2$ (M⁻¹ s⁻¹) 2Pyr₂ |
|---|---|---|---|
| UAMC-4129 | 0.76 | 4802 ± 693 | 184 892 ± 312 |
| UAMC-3933 | 2.96 | 3735 ± 323 | 87 265 ± 133 |
| UAMC-3711 | 1.58 | 2067 ± 224 | 91 460 ± 77 |
| UAMC-3724 | 1.71 | 4240 ± 102 | 146 200 ± 91 |
| UAMC-3725 | 1.92 | 3506 ± 311 | 142 626 ± 107 |

Figure S1). To compare the results with the literature, the d-TCOs were also reacted with 3,6-di-2-pyridyl-1,2,4,5-tetrazine (2Pyr₂) showing a remarkable rate constant in the range of 87 265−184 892 M⁻¹ s⁻¹ (Table 1; Table S1), which is in the similar range as previously reported d-TCO compounds.[9]

**Pretargeted Blocking.** A pretargeted blocking assay was established to assess the *in vivo* ligation performance of unlabeled d-TCO derivatives with Tz-modified antibodies (mAb-Tz) in tumor-bearing mice. The assay is based on the pretargeted blocking of ^{111}In-labeled-Tz as reported by Stéen et al. to identify the key parameters to obtain optimal Tz-based radiotracers.[12] Here, a Cy5-fluorophore-conjugated TCO was used together with a Tz-modified CC49 Ab (CC49-Tz) as a standard model for *in vivo* ligation. CC49 is a noninternalizing mAb that targets the tumor-associated glycoprotein-72 (TAG-72) which is overexpressed in a wide range of solid tumors, making it a perfect candidate for pretargeting. Based on previous reports, a pretargeting interval of 72 h was selected to maximize the clearance of unbound CC49-Tz from the circulation and to ensure lower background during imaging.[18] CC49 was modified with MeBA-NHS ester following a previously reported procedure yielding an average of 8-Tz bound to CC49 (Figure S2).[31] A binding assay was performed to confirm the conservation of the binding affinity of the mAb-Tz conjugate for the TAG-72 antigen when compared to the native CC49 Ab. CC49 ($K_d$ = 11.70 nM; 95% CI 9.91−13.49) and CC49-Tz ($K_d$ = 17.68 nM; 95% CI 8.42−26.94) both showed similar binding affinity toward human TAG-72 (Figure S3).

Through the blocking assay, the *in vivo* ligation efficiency of the unlabeled d-TCO derivatives can be inversely correlated to
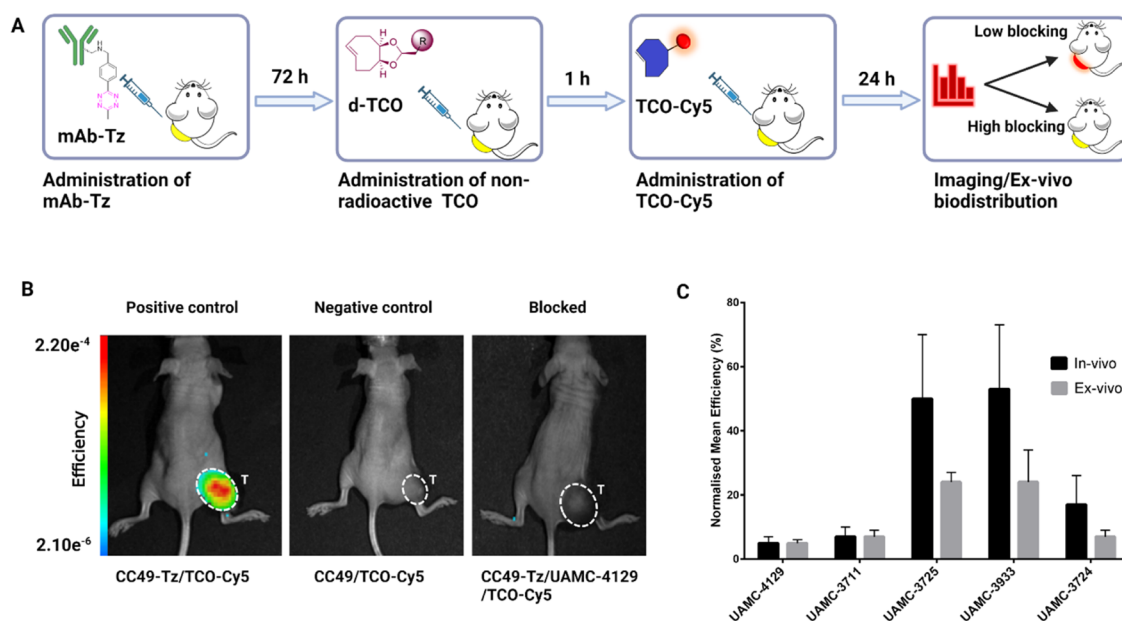
**Figure 1.** (A) Procedure followed for the *in vivo* pretargeted blocking approach. (B) *In vivo* representative fluorescence image of TCO-Cy5 uptake in LS174T tumor-bearing mice. Images were acquired 24 h post-TCO-Cy5 injection, and the fluorescence signal was quantified as total efficiency. The white dashed line encircles the tumor. (C) Tumor uptake of TCO-Cy5 *in vivo* and *ex vivo* was expressed as total efficiency in the blocked group. Data were normalized to TCO-Cy5 uptake in positive and negative control groups. (mean ± SD, $n$ = 4/group).

**Scheme 2. Precursor Synthesis and Radiosynthesis of [$^{18}$F]MICA-214 and [$^{18}$F]MICA-215**
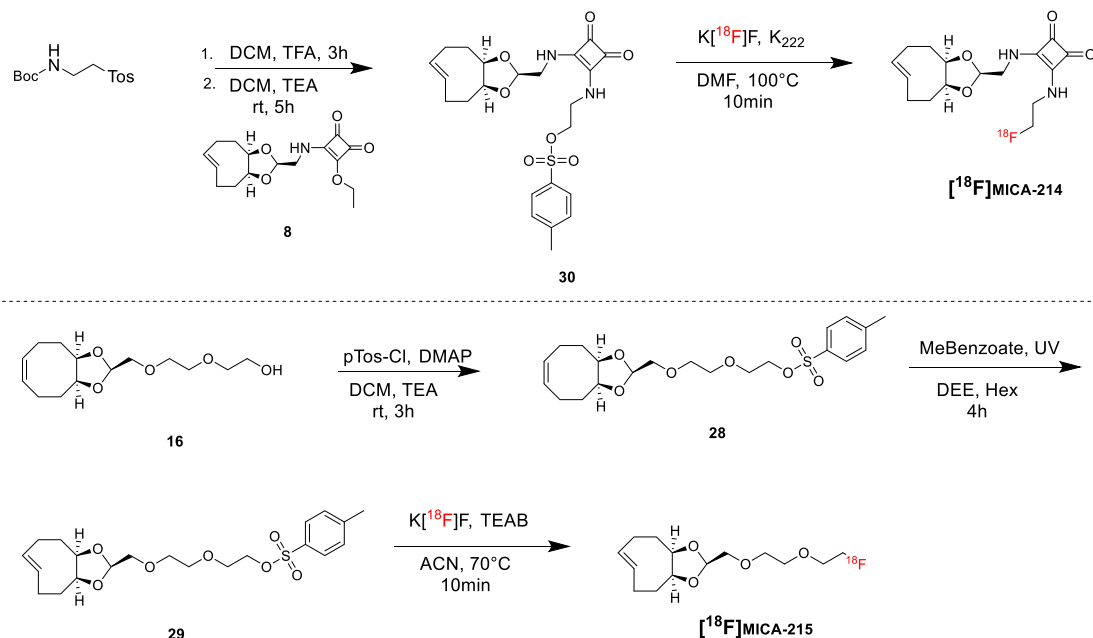


the uptake of TCO-Cy5 in the tumor (Figure 1A,B). The highest blocking efficiencies of 93 and 95% *in vivo* were observed for the d-TCO derivates **UAMC-3711** and **UAMC-4129** with the lowest uptake values of TCO-Cy5 in tumor 7 ± 3% ($n$ = 4) and 5 ± 2% ($n$ = 4), respectively. The *ex vivo* analysis also validated the findings from *in vivo* fluorescence measurements (Figure 1C). **UAMC-3724** showed moderate blocking efficiency with 17 ± 9% ($n$ = 4) of TCO-Cy5 uptake in the tumor, whereas **UAMC-3725** and **UAMC-3933** showed poor *in vivo* ligation performance with, respectively, higher TCO-Cy5 uptake values in tumor of 50 ± 20% ($n$ = 4) and 53 ± 20% ($n$ = 4). Given their high *in vivo* ligation efficiency,

**UAMC-4129** and **UAMC-3711** were chosen for further radiochemical development and evaluation.

**Radiochemistry.** For the synthesis of **MICA-214** precursor, 2-((tert-butoxycarbonyl)amino)ethyl 4-methylbenzene-sulfonate was first deprotected with trifluoroacetic acid (TFA) followed by the addition of **8** afforded the tosylate precursor **30**. Precursor **30** (6 mg) was reacted with K[$^{18}$F]F in DMF for 10 min at 100 °C to afford the radiolabeled product [$^{18}$F]MICA-214 (Scheme 2) in 5.2 ± 0.6% isolated radiochemical yield (RCY) decay-corrected to end of bombardment (EOB) with >98% radiochemical purity (RCP) and molar activity ($A_m$) between 36 and 50 GBq/μmol and a total
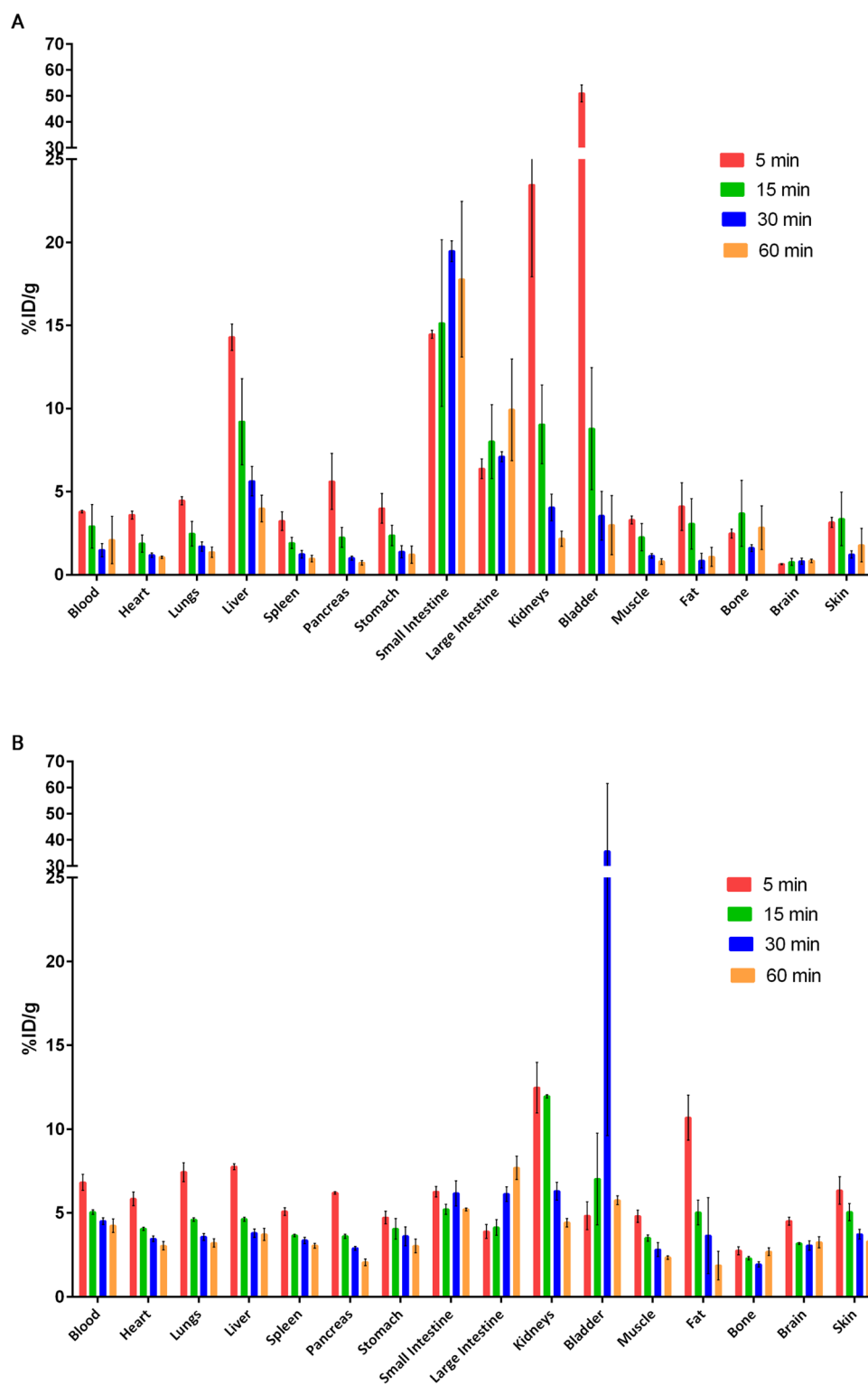
**Figure 2.** Biodistribution of (A) $[^{18}F]$**MICA-214** and (B) $[^{18}F]$**MICA-215** in naïve BALB/c mice (mean ± SD, $n$ = 3/group).

synthesis time of 60 min. **MICA-215** precursor was obtained by first tosylating **16** followed by the isomerization to trans-precursor **29**, which was reacted with $K[^{18}F]F$ in acetonitrile for 10 min at 100 °C to afford the radiolabeled product $[^{18}F]$**MICA-215** (Scheme 2) in 11.2 ± 0.4% isolated RCY (decay-corrected to EOB), with >98% RCP and $A_m \geq 7.34$ GBq/$\mu$mol and a total synthesis time of 72 min. The identity of both tracers was confirmed by coinjection and coelution of

the isolated radiotracers with the nonradiolabeled references **UAMC-4129** and **UAMC-3711** (Figure S4). Both radiotracers showed moderate lipophilicity with log $D$ values of 0.62 ± 0.09 ($n$ = 3) for $[^{18}F]$**MICA-214** and 1.25 ± 0.10 ($n$ = 3) for $[^{18}F]$**MICA-215**. The *in vitro* stability of both radiotracers was investigated by incubating the tracer in PBS at room temperature and mouse plasma at 37 °C. Both tracers showed excellent stability in PBS at 2 h with 93 ± 1.6% for
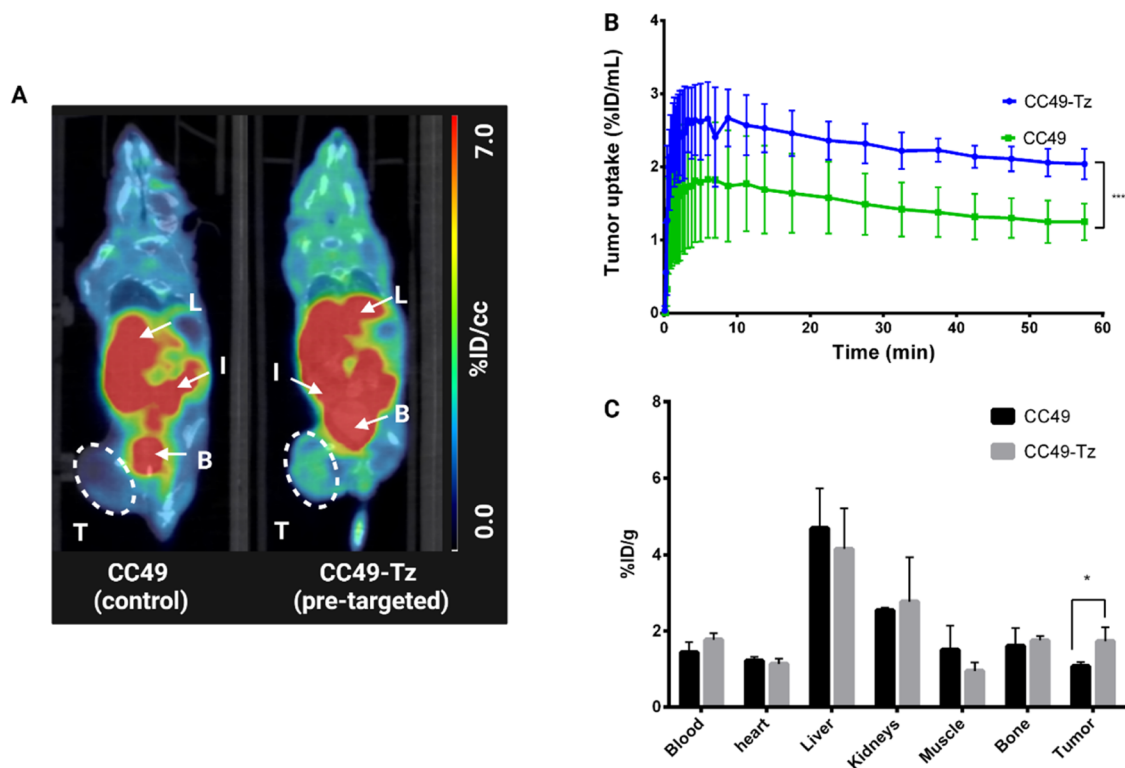
**Figure 3.** (A) *In vivo* representative coronal μPET/CT image of LS174T tumor-bearing mice injected with [¹⁸F]MICA-214 72 h post-CC49 (control) or CC49-Tz (pretargeted) injection. PET images represent the averaged tracer distribution from the dynamic scans (0−60 min). The white dashed lines encircle the tumor region, and the arrows represent the bladder (B), intestines (I), and liver (L). (B) Time−activity curve of tumor uptake of [¹⁸F]MICA-214 in groups injected with CC49-Tz and control group injected with CC49 (0 to 60 min) (mean ± SD, n = 4/group). (C) *Ex vivo* biodistribution of LS174T tumor-bearing mice 60 min post tracer injection.

[¹⁸F]MICA-214, and 100% intact tracer for [¹⁸F]MICA-15 (Figure S5). In plasma, 42 ± 2.9% (n = 3) of [¹⁸F]MICA-214 was available at 2 h (Figure S5), with the formation of one polar radiolabeled metabolite and a gradual increase of cis-isomer formation. In contrast, [¹⁸F]MICA-215 showed very good stability in plasma, with 94 ± 2.4% (n = 3) of intact radiotracer present at 2 h (Figure S5), and only a small amount of radiometabolites formation observed.

***Ex Vivo* Biodistribution and *In Vivo* Stability Studies in Non-Tumor-Bearing Mice.** Next, the pharmacokinetic profile and *in vivo* stability of the new d-TCO PET probes were evaluated in healthy mice (Figure 2; Tables S2 and S3; Figure S6). The *ex vivo* biodistribution of [¹⁸F]MICA-214 and [¹⁸F]MICA-215 showed mixed hepatobiliary and renal clearance of the radiotracer. For both tracers, the majority of the activity cleared through kidneys ([¹⁸F]MICA-214 2.2 ± 0.5% ID/g at 60 min; [¹⁸F]MICA-215 4.4 ± 0.2% ID/g at 60 min) followed by accumulation in the bladder and excretion in the urine ([¹⁸F]MICA-214 59.7 ± 15.1% ID/g at 60 min; [¹⁸F]MICA-215 606.3 ± 252.4%ID/g at 60 min). A smaller fraction of [¹⁸F]MICA-214 cleared through the liver ([¹⁸F]MICA-214 (4.0 ± 0.8% ID/g) at 60 min) with the highest accumulation in the small intestines ([¹⁸F]MICA-214 (17.8 ± 4.7% ID/g) at 60 min). In contrast, the uptake of [¹⁸F]MICA-215 in the small intestine remained lower ([¹⁸F]MICA-215 (5.2 ± 0.01% ID/g at 60 min)). Importantly, both tracers showed an absence of *in vivo* defluorination, with no significant increase in bone uptake ([¹⁸F]MICA-214 (2.8 ± 1.3% ID/g) at 60 min; [¹⁸F]MICA-215 2.7 ± 0.2%ID/g at 60 min). Overall, [¹⁸F]MICA-214 showed lower accumulation in remaining organs at 1 h p.i. compared to [¹⁸F]MICA-215

(Figure 2, Tables S2 and S3) and better renal clearance in comparison to previously reported d-TCO radiotracers.[22,26]

Both tracers were rapidly metabolized *in vivo* with 24.6 ± 2.4% (n = 3) of tracer remaining intact at 5 min and 10.8 ± 0.57% (n = 3) at 15 min for [¹⁸F]MICA-214. For [¹⁸F]MICA-215, 7.9 ± 2.3% (n = 3) and 2.1 ± 0.4% (n = 3) of radiotracer were intact at 5 and 15 min, respectively (Figure S6). In both cases, one prominent polar radiometabolite peak was observed, increasing over time up to 1 h p.i (92.0 ± 1.7% for [¹⁸F]MICA-214 and 95.1 ± 0.3% for [¹⁸F]MICA-215). Although the radiotracer is relatively rapidly metabolized *in vivo*, studies have shown that this only has a limited effect on the *in vivo* ligation due to the fast kinetics of the TCO-Tz reaction.[12] Nonetheless, the intact radiotracer must accumulate at the target site in sufficient quantities and react with the Tz-Ab conjugate to visualize the target. Due to the overall higher accumulation of [¹⁸F]MICA-215 combined with the faster *in vivo* metabolization of [¹⁸F]MICA-215 at earlier time points, its use *in vivo* is limited. Therefore, only [¹⁸F]MICA-214 was chosen for further pretargeted imaging studies in a tumor model.

***In Vivo* Pretargeted μPET Imaging.** Given the tracer's fast clearance, *in vivo* stability, low nonspecific tissue accumulation, and excellent *in vivo* ligation properties, we proceeded with pretargeted imaging in a tumor model using [¹⁸F]MICA-214. *In vivo*, pretargeted μPET imaging was performed in LS174T tumor-bearing mice pretreated with either CC49-Tz or CC49 (control group) 72 h before injection of [¹⁸F]MICA-214. The μPET images demonstrated an increased activity accumulation in the tumor in the group injected with CC49-Tz (2.16 ± 0.08% ID/mL). In contrast, in

the control group, the activity remained significantly lower ($1.34 \pm 0.07\%$ID/mL; $p < 0.0001$), which is consistent with the fact that there was no Tz tag present in the Ab (Figure 3A,3B). In accordance with the biodistribution studies in healthy mice, there were no differences in the uptake of radioactivity in other tissues between groups, indicating that CC49-Tz has been cleared from all nontarget tissues. *Ex vivo* biodistribution studies validated the *in vivo* results with significantly higher tumor uptake of [$^{18}$F]**MICA-214** in mice injected with CC49-Tz ($1.73 \pm 0.37\%$ID/g) than in the control group ($1.08 \pm 0.10\%$ID/g; $p = 0.0144$), as shown in Figure 3C (Table S4).

## ■ DISCUSSION

*In vivo*, pretargeted imaging relies highly on the stability and fast reaction kinetics between the reaction partners TCO and Tz. The d-TCO scaffold was selected due to its fast kinetics and enhanced stability compared to other strained TCO structures.[9] Compounds derivatized with short ethylene glycol chains were designed to increase hydrophilicity. A squaramide linker was chosen to impact both the hydrophilicity and the stability of the tracer. However, sulfonylamide and cyclopropyl linkers were chosen to impact the $^{18}$F−C bond stability.[30] For the synthesis of the d-TCO derivatives, mild reaction conditions were chosen to avoid trans to cis isomerization during synthesis. Where possible, the compounds were isomerized at the final stage of synthesis.

The synthesized compounds were tested for their reactivity against tetrazine. As we inverted the functionalities, the stability of the Tz conjugated to mAb rather than just the ultrafast kinetics plays a significant role. 6-Methylated tetrazines are known to be more stable in exposure to physiological conditions.[32] Hence, MeBA was selected as the model Tz for *in vivo* ligation based on the literature regarding its use in biological applications, stability, and commercial availability. MeBA with its remarkable stability and moderate kinetics is currently, to the best of our knowledge, the only tetrazine in use in a human clinical trial for pretargeted drug delivery.[33,34] Only slight differences in the reactivity of d-TCOs with different linkers were observed, as the linkers are distant from the reaction center of the dienophile. Compounds with more hydrophilic linkers exhibited slightly faster kinetics. The kinetics of the synthesized d-TCOs are also comparable to previously reported d-TCO derivatives.[22,26] The overall reactivity remained similar to the parent d-TCO compound with $k_2$ of $167\,000 \pm 7000$ M$^{-1}$ s$^{-1}$ in similar reaction conditions.

To assess the *in vivo* ligation of the synthesized compounds, a pretargeted blocking assay was developed. This screening assay allowed us to have an earlier readout of the TCO reactivity toward Ab-modified Tz, avoiding the need for time-consuming radiochemical development of each TCO derivative. Compounds UAMC-3711 and UAMC-4129 containing polar linkers (squaramide and PEG chain) showed excellent blocking efficiency. In contrast, compounds containing more lipophilic cyclobutyl fluoride and 6-fluoro-3-sulfonylpyridine linkers and with higher $\log D$ values showed poor blocking efficiency. Nonetheless, bigger compound libraries are required to establish a more profound correlation.

The radiolabeling conditions differed slightly for both tracers. In the case of [$^{18}$F]**MICA-214**, better radiochemical conversion (RCC) was achieved with Kryptofix$_{2.2.2}$ (K$_{2.2.2}$) when compared to that with tetraethylammonium bicarbonate

(TEAB). On the other hand, TEAB provided sufficient RCC for [$^{18}$F]**MICA-215**. TCOs are known to isomerize at higher temperatures.[35] Here, a larger disparity in temperature tolerance was observed. Only a negligible amount of trans-to-cis isomerization was observed for [$^{18}$F]**MICA-214** up to 100 °C. However, only the cis-isomer of [$^{18}$F]**MICA-215** was isolated at temperatures above 80 °C. Also, the choice of solvent played a role. In both cases, only cis-isomers were observed when reactions were performed in DMSO. The RCC for both tracers was satisfactory, and isolated RCY of both tracers remained relatively low due to some trans-to-cis isomerization of both precursors and products during radiosynthesis. Nonetheless, the reported RCYs are comparable to previously reported $^{18}$F-labeled d-TCOs.[21,22,26]

*In vitro*, [$^{18}$F]**MICA-215** exhibited superior stability compared to [$^{18}$F]**MICA-214**. However, the situation was reversed *in vivo*, with [$^{18}$F]**MICA-214** demonstrating a higher stability than [$^{18}$F]**MICA-215**. This finding emphasizes the importance of conducting *in vivo* stability assessments rather than relying solely on extrapolating data from plasma stability screenings.

In biodistribution studies, both tracers displayed mixed renal and hepatobiliary clearance resulting in high abdominal activity as observed for previously described d-TCO radiotracers.[22,26] [$^{18}$F]**MICA-214** showed faster renal clearance when compared to [$^{18}$F]**MICA-215** with higher radioactivity accumulation in kidneys and bladder at earlier time points (Figure 2). Higher radioactivity accumulation in intestines is observed with [$^{18}$F]**MICA-214** ($17.8 \pm 4.7\%$ ID/g at 60 min) compared to [$^{18}$F]**MICA-215** ($5.2 \pm 0.01\%$ ID/g at 60 min), indicating that the accumulation might be associated with linker dependent metabolization of the compound. Thus, further fine-tuning of the linker with polar groups to decrease the liver clearance could reduce abdominal activity. Furthermore, the *in vivo* stability assessment of [$^{18}$F]**MICA-214** and [$^{18}$F]**MICA-215** showed substantial metabolization of the radiotracers (Figure S6). Thus, the higher accumulation of radioactivity can also be attributed to the accumulation of radiometabolites in these organs. In both instances, HPLC analysis revealed the presence of a polar radiometabolite. Among the potential metabolites that may be formed *in vivo*, one could be the free aldehyde with an $^{18}$F-label on the linker, resulting from the hydrolysis of the dioxolane ring of the d-TCO. Several strategies have been proposed in the literature to stabilize the acetal group *in vivo*, such as the introduction of proximal electron-withdrawing groups, basic amines, heteroaryl rings, or the implementation of steric and strain effects.[36] Nevertheless, further detailed analyses and investigations are imperative to substantiate this hypothesis. During the pretargeted imaging study, the radioactivity in the blood remained similar to the biodistribution studies, suggesting the [$^{18}$F]**MICA-214** is primarily reacting with CC49-Tz at the tumor site rather than with mAb still circulating in the blood implying a good pretargeting interval between the mAb-Tz and the radiotracer injection.[12,14] Both *in vivo* PET/CT data and *ex vivo* analysis showed a significantly higher tumor uptake compared to the control group confirming the *in vivo* d-TCO-Tz ligation. The main obstacle remains the high abdominal uptake as seen with previously developed d-TCO derivatives.[25,26] When compared with $^{18}$F-labeled Tzs, a low tumor-to-muscle (T/M) ratio of 1.8 was observed (Table S4). However, with a tumor-to-blood (T/B) ratio of 0.9 and tumor-to-liver ratio of 0.4 (Table S4), the target-to-background contrast remained comparable to

previously reported studies with $^{18}$F-labeled Tzs.[11,13,14] This emphasizes the general need to improve tumor-to-background ratios in pretargeted imaging studies. Further optimization of the tracer with more polar linkers containing longer PEG chains or introduction of diacetic acid or sugar molecules could increase the TCO's polarity enhancing the real clearance while decreasing nonspecific uptake. Additionally, the use of more hydrophilic-TCO variants, like oxo-TCO, could offer an alternative.[37] Finally, the identification of metabolites could guide the design of TCOs toward more metabolically stable compounds. These combined factors might decrease the uptake of the tracer in nontarget tissues to reduce the background signal, which led to low tumor-to-background ratios.

## ■ CONCLUSIONS

Pretargeted PET imaging is a promising approach for the development of precision and highly efficient tools for personalized diagnostics and safe radionuclide therapy treatment of patients. Despite recent progress in the field, the development and availability of radiolabeled compounds for in vivo use remain quite limited. Bigger libraries of the compound and systematic studies are needed to gain further insight into the pretargeting approach to pave the way toward clinical translation. In an effort to expand the bioorthogonal toolbox, we have developed a diverse series of d-TCO probes with excellent reactivity toward tetrazines and evaluated their in vivo ligation ability through a pretargeted blocking approach. From the series, the best-performing compounds were selected for further radiochemical development, pharmacokinetics, and in vivo stability evaluation. Finally, the radiotracer [$^{18}$F]MICA-214 was used in pretargeted PET imaging in mice bearing tumors. Although higher activity accumulation of the radiotracer was achieved in the mice injected with CC49-Tz compared with the control group, further optimization of the radiotracer is needed to reduce background uptake, and thus enhance tumor contrast in future studies. Nevertheless, this work creates a base for further development and evaluation of d-TCO-based radiotracers for pretargeted PET imaging.

## ■ MATERIALS AND METHODS

**General.** All chemicals, reagents, and solvents were purchased from commercial suppliers (Sigma-Aldrich, Acros, TCI-Europe, FluoroChem, BioRad, and Jena Bioscience) and used without further purification. Phosphate-buffered saline (PBS, 0.01 M, pH 7.4) solutions were obtained by diluting a 0.5 M stock purchased from Gentest Life Technology.

NMR spectra were recorded on a Bruker Avance DRX 400 MHz spectrometer. $^{1}$H and $^{13}$C spectra are referenced to residual solvent peaks, and coupling constants are given in hertz. HRMS analyses were performed using a Q-TOF II instrument (Waters, Manchester, U.K.). UPLC-MS analyses were performed on a Waters Acquity UPLC system coupled to a Waters TQD ESI mass spectrometer and TUV detector. Kinetics were performed on an SX-20 stopped-flow system (Applied Photophysics). log $D$ values were calculated with Collaborative Drug Vault. Chromatographic purifications were performed with a Biotage ISOLERA One flash system equipped with an internal variable dual-wavelength diode array detector (200−400 nm).

**Stopped-Flow Kinetics.** The reaction between d-TCOs and the tetrazines was measured under pseudo-first-order conditions in water/methanol 50:50 with excess TCO by following the exponential decay of the MeBA-Tz at 264 nm and 2Pyr$_2$-Tz at 300 nm over time using an SX 20 stopped-flow spectrophotometer (Applied Photophysics Ltd.). The solutions were thermostated in the syringes of the spectrophotometer before measuring. An equal volume of each was mixed by the stopped-flow device, and 4000 data points were recorded over a period of 20 s and performed in quadruplicate at 37 °C. Data were analyzed by fitting an exponential decay using GraphPad Prism version 9.3.1 (RRID: SCR_002798), and the obtained kobs were plotted vs TCO concentration using nonlinear regression to afford the second-order constant ($k_2$), based on the equation kobs = [TCO] $k_2$ for MeBA (Figure S1). For 2Pyr$_2$, pseudo-first-order rate constants were divided by the TCO concentration to calculate the second-order rate constants (Table S1).

**Blocking Studies.** *Animal Model.* The in vivo experiments were performed in tumor-bearing female nude Balb/C mice (6−8 weeks old, Charles River Laboratories). The mice were kept under environmentally controlled conditions (12 h light/dark cycle, 20−24 °C, and 40−70% relative humidity) in IVC cages with food and water ad libitum. The human colon cancer cell line LS174T (ATCC CL-188) was obtained from the ATCC. Cells were maintained in DMEM (Sigma) supplemented with 10% fetal bovine serum, 2 mM L-glutamine, 1 mM sodium pyruvate, and 1% penicillin-streptomycin (Invitrogen) at 37 °C and 5% $CO_2$.

The xenograft model was generated by subcutaneous injection of LS174T ($5 \times 10^6$ viable cells in 100 $\mu$L of Dulbecco phosphate-buffered saline, DPBS) tumor cells into the right hind flank of 6- to 8-week-old female Balb/C nude mice. After tumor inoculation, tumor dimensions were measured using a digital caliper three times over a week. Tumor volumes were calculated according to the formula (length x width$^2$)/2. At the end of each experiment, the mice were euthanized by cervical dislocation. All experimental procedures and protocols were performed following European Directive 86/609/EEC Welfare and Treatment of Animals and were approved by the local ethical commission (2018−87, University of Antwerp, Belgium).

*In Vivo Fluorescence Imaging.* For the positive and negative control group, nude female Balb/C LS174T tumor-bearing mice (n = 4) were either injected with CC49-Tz (100 $\mu$g/100 $\mu$L, 0.67 nmol) or CC49 (100 $\mu$g/100 $\mu$L, 0.67 nmol) 72 h before TCO-Cy5 (40 nmol/100 $\mu$L) injection. Mice in the blocked group were injected with CC49-Tz 72h before the unlabeled d-TCO derivatives (40 nmol/100 $\mu$L) followed by TCO-Cy5 (40 nmol/100 $\mu$L) after 1 h (Figure 1A). The mice were anesthetized with 2.5% isoflurane (IsoFlo, Zoetis) for 3 min in an induction chamber. Upon induction, the mice were transferred to the IVIS Spectrum *in vivo* Imaging System (PerkinElmer) and imaged. Image sequences were acquired with the same exposure time, binning, and F-stop values. Images were analyzed, and the tumor uptake of TCO-Cy5 was quantified by drawing the region of interest (ROI) using Aura V3.2 (Spectral Instruments Imaging). The uptake value of the positive control group was used as a reference value (100% tumor uptake). The uptake value of the negative group was used to determine the background signal (0% tumor uptake). These reference values were used to normalize the observed tumor uptake in groups with a blocking experiment. Tumor uptake of the blocked group is presented as a percentage normalized mean efficiency (Figure 1).

*Radiochemistry.* The radiosynthesis was carried out in an automated AllinOne synthesis module (TRASIS, Ans, Belgium) with an integrated HPLC system with a UV detector and a radioactivity detector. No-carrier added aqueous $[^{18}F]$ fluoride was produced in an Eclipse HP cyclotron (Siemens) using the $^{18}O(p,n)^{18}F$ reaction by proton bombardment of $[^{18}O]H_2O$ (Rotem Industries), and passed through an ion-exchange resin (Sep-Pak Accell Plus QMA Light cartridge (Waters)). $[^{18}F]F^-$ was eluted from the resin in the reactor vial with 1 mL of a mixture of 0.025 M $K_2CO_3$/0.1 M kryptofix$_{2.2.2}$ in $CH_3CN/H_2O$ (95:5 (v/v)) for $[^{18}F]MICA-214$ and 0.01 M tetraethylammonium bicarbonate (TEAB) in $CH_3CN/H_2O$ (90:10 (v/v)) for $[^{18}F]MICA-215$, and evaporated to dryness. For $[^{18}F]MICA-214$, a tosylate precursor solution (6 mg) in dry DMF was added and reacted for 10 min at 100 °C, and for $[^{18}F]MICA-215$, a tosylate precursor (5 mg) in dry ACN was added and reacted for 10 min at 70 °C. After cooling down to 50 °C, 1 mL of buffer was added and the mixture was passed through a Sep-Pak Alumina N Light cartridge (Waters) (preconditioned with 10 mL of water), before injection on the HPLC. $[^{18}F]MICA-214$ was purified using a Waters X-Bridge C18 250 × 10 mm (5 μm) HPLC column using a mobile phase consisting of NaOAc 0.05 M pH 5.5/EtOH (70:30 (v/v)) at a flow rate of 3 mL/min ($[^{18}F]MICA-214$ $t_R$ = 18 min). $[^{18}F]MICA-215$ was purified using a Phenomenex Luna C18 250 × 10 mm (5 μm) HPLC column using a mobile phase NaOAc 0.05 M pH 5.5/EtOH (60:40 (v/v)) at a flow rate of 3 mL/min ($[^{18}F]MICA-215$ $t_R$ = 28 min). Radiotracers were sterile-filtered and diluted with 0.9% NaCl to reduce ethanol concentration to <10% in the final formulation. Radiochemical purity was determined by analytical reversed-phase HPLC using a Phenomenex Kinetex EVO C18 150 mm × 4.6 mm (5 μm) with an isocratic elution of $H_2O$ + 0.1% TFA/$CH_3CN$ + 0.1% TFA (72:28) over 10 min for $[^{18}F]MICA-214$; and $H_2O$ + 0.1% TFA/$CH_3CN$ + 0.1% TFA (70:30) over 15 min for $[^{18}F]MICA-215$, with a flow rate of 1 mL/min (Figure S4). The recorded data were processed by the GINA-Star 5 software (Raytest). Radiochemical yields (RCY) were calculated from the theoretical initial amount of $[^{18}F]F^-$ and decay was corrected to the end of bombardment (EOB).

*Partition Coefficient Determination.* The partition coefficient ($\log D_{\text{n-octanol/PBS pH 7.4}}$) of $[^{18}F]MICA-214$ and $[^{18}F]MICA-215$ was measured using the "shake-flask" method. Briefly, approximately 74 kBq of $[^{18}F]MICA-214$ or $[^{18}F]MICA-215$ was added to a test tube containing a mixture of 2 mL of n-octanol and 2 mL of PBS (0.01 M, pH 7.4). The mixture was shaken well, vortexed for 2 min, and centrifuged at 3000 rpm for 10 min. After the separation of the layers, a 0.5 mL aliquot of both layers was taken into separate tubes and counted for radioactivity in an automatic gamma-($\gamma$) counter (Wizard2 2480, PerkinElmer). Corrections were made for differences in mass and density between the two phases. The octanol−water partition coefficients were obtained by dividing the octanol-containing radioactivity by the PBS-containing radioactivity, and the $\log_{10}$ of this ratio was calculated. Reported $\log D$ values represent the mean of three determinations and were expressed as mean ± standard deviation (SD).

*In Vitro Stability Evaluation.* The stabilities of $[^{18}F]MICA-214$ and $[^{18}F]MICA-215$ were evaluated in PBS (0.01 M, pH 7.4) and mouse plasma at 37 °C for up to 120 min. Approximately, 185−370 kBq of $[^{18}F]MICA-214$ or

$[^{18}F]MICA-215$ was incubated in 100 μL of PBS or mouse plasma. The incubation was quenched by adding ice-cold ACN (100 μL), followed by vortexing and centrifugation (5 min, 4000$g$) to remove the proteins from samples in plasma. The radioactive contents of the supernatant (100 μL) were analyzed by analytical radio-HPLC. The HPLC eluate was collected in fractions of 15 s, and the radioactivity was counted in an automated $\gamma$-counter.

*Ex Vivo Biodistribution Studies.* Female nude Balb/C healthy and LST174 tumor-bearing mice were intravenously administered with $[^{18}F]MICA-214$ or $[^{18}F]MICA-215$ approximately 5 MBq per mouse, $n$ = 3/time point via the lateral tail vein. At 5, 15, 30, and 60 min post-radiotracer injection (p.i.), the blood was collected through cardiac puncture and the mice were euthanized by cervical dislocation. The selected organs and tissues were harvested, weighed, and blotted dry. The sample radioactivity was counted in a $\gamma$-counter (Wizard$^2$ 2480, PerkinElmer) and the uptake of radiotracer is presented as the injected dose per gram (%ID/g).

*In Vivo Metabolite Analysis.* The blood from the *ex vivo* biodistribution studies was collected in EDTA-coated tubes. The plasma fraction was obtained by centrifugation at 4000$g$ for 7 min and mixed (200 μL) with an equal volume of ice-cold ACN to enable deproteination. The samples were centrifuged at 4000$g$ for 4 min, and the supernatant and pellet were $\gamma$-counted separately. The radioactive contents of the supernatant (100 μL) were analyzed by analytical radio-HPLC. The HPLC eluate was collected in fractions of 15 s, and the radioactivity was counted in an automated $\gamma$-counter.

*In Vivo μPET Imaging Studies.* Nude female Balb/C mice bearing LS174T tumors ($n$ = 4) were anesthetized using isoflurane (5% for induction, 2% for maintenance), placed on the animal bed in the scanner, and i.v. injected via lateral tail vein with 8−9 MBq of $[^{18}F]MICA-214$. Dynamic whole-body PET images were acquired for 60 min (12 × 10 s, 3 × 20 s, 3 × 30 s, 3 × 60 s, 3 × 150 s, and 9 × 300 s frames), using an Inveon small animal PET-CT scanner (Siemens). After each PET acquisition, a whole-body CT scan was performed to obtain anatomic information for segmentation. The mice were maintained at a constant body temperature throughout the PET-CT scanning procedure using a heating pad. For quantitative analysis, PET data were reconstructed using a list-mode iterative reconstruction with proprietary spatially variant resolution modeling in 8 iterations and 16 subsets of the 3D ordered subset expectation maximization (OSEM 3D) algorithm.[38] The PET images were additionally reconstructed on a 128 × 128 × 159 matrix with a voxel size of 0.776 × 0.776 × 0.776 mm. CT-based attenuation and single scatter stimulation (SSS) scatter corrections were applied to the PET data. For the dynamic scans, volumes of interest (VOIs) were manually drawn on the PET/CT images using PMOD (version 3.6; PMOD Technologies) to delineate the regions with distinct PET time−activity patterns: heart, liver, kidney, bladder, muscle, brain, bone, and tumor. The average organ activity per volume was obtained from the coregistered PET images, and the decay-corrected time−activity curves (TACs) were extracted for each target organ. For an absolute measure of tracer uptake in the tissue, normalized images were scaled according to the percent-injected dose (%ID/mL = tissue uptake from the scanner [kBq/mL]/injected dose [kBq] x 100).

*Data Analysis.* Data were expressed as mean ± SD. Statistical analysis was performed using GraphPad Prism

version 9.3.1 (RRID: SCR_002798). Statistical significance between the two data sets was evaluated by the unpaired two-tailed Student $t$ test. Differences between groups were considered statistically significant if the p value was less than 0.05.

## ASSOCIATED CONTENT

### Ⓢ Supporting Information

The Supporting Information is available free of charge at https://pubs.acs.org/doi/10.1021/acsomega.3c04597.

General experimental and equipment information, chemical structures, synthesis and additional data of all precursor molecules, kinetic rates data, antibody production and conjugation data, representative radio-HPLC traces, in vitro and in vivo stability data, and ex vivo biodistribution data (PDF)

## AUTHOR INFORMATION

### Corresponding Authors

**Filipe Elvas** − Department of Nuclear Medicine, Antwerp University Hospital, Edegem 2650, Belgium; Molecular Imaging Center Antwerp, University of Antwerp, Antwerp 2610, Belgium; ⓞ orcid.org/0000-0001-9790-3369; Email: Filipe.Elvas@uantwerpen.be

**Koen Augustyns** − Laboratory of Medicinal Chemistry, University of Antwerp, Antwerp 2610, Belgium; ⓞ orcid.org/0000-0002-5203-4339; Email: Koen.Augustyns@uantwerpen.be

### Authors

**Karuna Adhikari** − Laboratory of Medicinal Chemistry, University of Antwerp, Antwerp 2610, Belgium; ⓞ orcid.org/0000-0002-5036-0616

**Jonatan Dewulf** − Molecular Imaging Center Antwerp, University of Antwerp, Antwerp 2610, Belgium; ⓞ orcid.org/0000-0003-0697-7667

**Christel Vangestel** − Department of Nuclear Medicine, Antwerp University Hospital, Edegem 2650, Belgium; Molecular Imaging Center Antwerp, University of Antwerp, Antwerp 2610, Belgium

**Pieter Van der Veken** − Laboratory of Medicinal Chemistry, University of Antwerp, Antwerp 2610, Belgium; ⓞ orcid.org/0000-0003-1208-3571

**Sigrid Stroobants** − Department of Nuclear Medicine, Antwerp University Hospital, Edegem 2650, Belgium; Molecular Imaging Center Antwerp, University of Antwerp, Antwerp 2610, Belgium

Complete contact information is available at:
https://pubs.acs.org/10.1021/acsomega.3c04597

### Notes

The authors declare no competing financial interest.

## ACKNOWLEDGMENTS

## ABBREVIATIONS

IEDDA:inverse electron demand Diels−Alder
Tz:tetrazine
TCO:trans-cyclooctene
PET:positron emission tomography
Immuno-PET:immuno-positron emission tomography
mAbs:monoclonal antibodies
sTCO:strained cyclopropane-fused TCO
d-TCO:cis-dioxolane-fused TCO
PEG:poly(ethylene glycol)
PBSF:perfluoro-1-butanesulfonyl fluoride
MeBA:6-methylbenzylamine tetrazine
2Pyr$_2$:3,6-di-2-pyridyl-1,2,4,5-tetrazine
TFA:trifluoroacetic acid
DMF:dimethylformamide
K222:Kryptofix 2.2.2
RCY:radiochemical yield
EOB:end of bombardment
$A_m$:molar activity

## REFERENCES

(1) Rondon, A.; Degoul, F. Antibody Pretargeting Based on Bioorthogonal Click Chemistry for Cancer Imaging and Targeted Radionuclide Therapy. Bioconjugate Chem. 2020, 31 (2), 159−173.

(2) Stéen, E. J. L.; Edem, P. E.; Norregaard, K.; Jorgensen, J. T.; Shalgunov, V.; Kjaer, A.; Herth, M. M. Pretargeting in nuclear imaging and radionuclide therapy: Improving efficacy of theranostics and nanomedicines. Biomaterials 2018, 179, 209−245.

(3) Hapuarachchige, S.; Artemov, D. Theranostic Pretargeting Drug Delivery and Imaging Platforms in Cancer Precision Medicine. Front. Oncol. 2020, 10, 1131.

(4) Wei, W.; Rosenkrans, Z. T.; Liu, J.; Huang, G.; Luo, Q. Y.; Cai, W. ImmunoPET: Concept, Design, and Applications. Chem. Rev. 2020, 120 (8), 3787−3851.

(5) Meyer, J. P.; Houghton, J. L.; Kozlowski, P.; Abdel-Atti, D.; Reiner, T.; Pillarsetty, N. V.; Scholz, W. W.; Zeglis, B. M.; Lewis, J. S. ^{18}F-Based Pretargeted PET Imaging Based on Bioorthogonal Diels-Alder Click Chemistry. Bioconjugate Chem. 2016, 27 (2), 298−301.

(6) Altai, M.; Membreno, R.; Cook, B.; Tolmachev, V.; Zeglis, B. M. Pretargeted Imaging and Therapy. J. Nucl. Med. 2017, 58 (10), 1553−1559.

(7) Miller, P. W.; Long, N. J.; Vilar, R.; Gee, A. D. Synthesis of ^{11}C, ^{18}F, ^{15}O, and [13]N Radiolabels for Positron Emission Tomography. Angew. Chem., Int. Ed. 2008, 47 (47), 8998−9033.

(8) Devaraj, N. K.; Thurber, G. M.; Keliher, E. J.; Marinelli, B.; Weissleder, R. Reactive polymer enables efficient in vivo bioorthogonal chemistry. Proc. Natl. Acad. Sci. U.S.A. 2012, 109 (13), 4762−4767.

(9) Darko, A.; Wallace, S.; Dmitrenko, O.; Machovina, M. M.; Mehl, R. A.; Chin, J. W.; Fox, J. M. Conformationally Strained trans-Cyclooctene with Improved Stability and Excellent Reactivity in Tetrazine Ligation. Chem. Sci. 2014, 5 (10), 3770−3776.

(10) Keinänen, O.; Li, X.-G.; Chenna, N. K.; Lumen, D.; Ott, J.; Molthoff, C. F. M.; Sarparanta, M.; Helariutta, K.; Vuorinen, T.; Windhorst, A. D.; Airaksinen, A. J. A New Highly Reactive and Low Lipophilicity Fluorine-18 Labeled Tetrazine Derivative for Pretargeted PET Imaging. ACS Med. Chem. Lett. 2016, 7 (1), 62−66.

(11) Battisti, U. M.; Bratteby, K.; Jørgensen, J. T.; Hvass, L.; Shalgunov, V.; Mikula, H.; Kjær, A.; Herth, M. M. Development of the First Aliphatic ^{18}F-Labeled Tetrazine Suitable for Pretargeted PET Imaging—Expanding the Bioorthogonal Tool Box. J. Med. Chem. 2021, 64 (20), 15297−15312.

(12) Stéen, E. J. L.; Jørgensen, J. T.; Denk, C.; Battisti, U. M.; Nørregaard, K.; Edem, P. E.; Bratteby, K.; Shalgunov, V.; Wilkovitsch, M.; Svatunek, D.; Poulie, C. B. M.; Hvass, L.; Simón, M.; Wanek, T.; Rossin, R.; Robillard, M.; Kristensen, J. L.; Mikula, H.; Kjaer, A.;

Herth, M. M. Lipophilicity and Click Reactivity Determine the Performance of Bioorthogonal Tetrazine Tools in Pretargeted In Vivo Chemistry. *ACS Pharmacol. Transl. Sci.* **2021**, *4* (2), 824−833.

(13) García-Vázquez, R.; Battisti, U. M.; Jørgensen, J. T.; Shalgunov, V.; Hvass, L.; Stares, D. L.; Petersen, I. N.; Crestey, F.; Löffler, A.; Svatunek, D.; Kristensen, J. L.; Mikula, H.; Kjaer, A.; Herth, M. M. Direct Cu-mediated aromatic $^{18}$F-labeling of highly reactive tetrazines for pretargeted bioorthogonal PET imaging. *Chem. Sci.* **2021**, *12* (35), 11668−11675.

(14) García-Vázquez, R.; Jørgensen, J. T.; Bratteby, K. E.; Shalgunov, V.; Hvass, L.; Herth, M. M.; Kjær, A.; Battisti, U. M. Development of $^{18}$F-Labeled Bispyridyl Tetrazines for In Vivo Pretargeted PET Imaging. *Pharmaceuticals* **2022**, *15* (2), 245 DOI: 10.3390/ph15020245.

(15) Poulie, C. B. M.; Jørgensen, J. T.; Shalgunov, V.; Kougioumtzoglou, G.; Jeppesen, T. E.; Kjaer, A.; Herth, M. M. Evaluation of [$^{64}$Cu]Cu-NOTA-PEG$_7$-H-Tz for Pretargeted Imaging in LS174T Xenografts-Comparison to [$^{111}$In]In-DOTA-PEG$_{11}$-BisPy-Tz. *Molecules* **2021**, *26* (3), 544 DOI: 10.3390/molecules26030544.

(16) Edem, P. E.; Sinnes, J.-P.; Pektor, S.; Bausbacher, N.; Rossin, R.; Yazdani, A.; Miederer, M.; Kjær, A.; Valliant, J. F.; Robillard, M. S.; Rösch, F.; Herth, M. M. Evaluation of the inverse electron demand Diels-Alder reaction in rats using a scandium-44-labelled tetrazine for pretargeted PET imaging. *EJNMMI Res.* **2019**, *9* (1), 49.

(17) Rahim, M. K.; Kota, R.; Haun, J. B. Enhancing Reactivity for Bioorthogonal Pretargeting by Unmasking Antibody-Conjugated trans-Cyclooctenes. *Bioconjugate Chem.* **2015**, *26* (2), 352−360.

(18) Rossin, R.; van den Bosch, S. M.; ten Hoeve, W.; Carvelli, M.; Versteegen, R. M.; Lub, J.; Robillard, M. S. Highly Reactive trans-Cyclooctene Tags with Improved Stability for Diels−Alder Chemistry in Living Systems. *Bioconjugate Chem.* **2013**, *24* (7), 1210−1217.

(19) wyffels, L.; Thomae, D.; Waldron, A.-M.; Fissers, J.; Dedeurwaerdere, S.; Van der Veken, P.; Joossens, J.; Stroobants, S.; Augustyns, K.; Staelens, S. In vivo evaluation of $^{18}$F-labeled TCO for pre-targeted PET imaging in the brain. *Nucl. Med. Biol.* **2014**, *41* (6), 513−523.

(20) Li, Z.; Cai, H.; Hassink, M.; Blackman, M. L.; Brown, R. C.; Conti, P. S.; Fox, J. M. Tetrazine-trans-cyclooctene ligation for the rapid construction of $^{18}$F labeled probes. *Chem. Commun.* **2010**, *46* (42), 8043−8045.

(21) Ruivo, E.; Adhikari, K.; Elvas, F.; Fissers, J.; Vangestel, C.; Staelens, S.; Stroobants, S.; Van der Veken, P.; Wyffels, L.; Augustyns, K. Improved stability of a novel fluorine-18 labeled TCO analogue for pretargeted PET imaging. *Nucl. Med. Biol.* **2019**, *76−77*, 36−42.

(22) Billaud, E. M. F.; Shahbazali, E.; Ahamed, M.; Cleeren, F.; Noël, T.; Koole, M.; Verbruggen, A.; Hessel, V.; Bormans, G. Micro-flow photosynthesis of new dienophiles for inverse-electron-demand Diels−Alder reactions. Potential applications for pretargeted in vivo PET imaging. *Chem. Sci.* **2017**, *8* (2), 1251−1258.

(23) Taylor, M. T.; Blackman, M. L.; Dmitrenko, O.; Fox, J. M. Design and Synthesis of Highly Reactive Dienophiles for the Tetrazine−trans-Cyclooctene Ligation. *J. Am. Chem. Soc.* **2011**, *133* (25), 9646−9649.

(24) Wang, M.; Svatunek, D.; Rohlfing, K.; Liu, Y.; Wang, H.; Giglio, B.; Yuan, H.; Wu, Z.; Li, Z.; Fox, J. Conformationally Strained trans-Cyclooctene (sTCO) Enables the Rapid Construction of $^{18}$F-PET Probes via Tetrazine Ligation. *Theranostics* **2016**, *6* (6), 887−895.

(25) Billaud, E. M. F.; Belderbos, S.; Cleeren, F.; Maes, W.; Van de Wouwer, M.; Koole, M.; Verbruggen, A.; Himmelreich, U.; Geukens, N.; Bormans, G. Pretargeted PET Imaging Using a Bioorthogonal $^{18}$F-Labeled trans-Cyclooctene in an Ovarian Carcinoma Model. *Bioconjugate Chem.* **2017**, *28* (12), 2915−2920.

(26) Ruivo, E.; Elvas, F.; Adhikari, K.; Vangestel, C.; Van Haesendonck, G.; Lemiere, F.; Staelens, S.; Stroobants, S.; Van der Veken, P.; Wyffels, L.; Augustyns, K. Preclinical Evaluation of a Novel $^{18}$F-Labeled dTCO-Amide Derivative for Bioorthogonal Pretargeted Positron Emission Tomography Imaging. *ACS Omega* **2020**, *5* (9), 4449−4456.

(27) van der Kolk, M. R.; Janssen, M.; Rutjes, F.; Blanco-Ania, D. Cyclobutanes in Small-Molecule Drug Candidates. *ChemMedChem.* **2022**, *17* (9), No. e202200020.

(28) Molineux, G. Pegylation: engineering improved pharmaceuticals for enhanced therapy. *Cancer Treat Rev.* **2002**, *28*, 13−16.

(29) Marchetti, L. A.; Kumawat, L. K.; Mao, N.; Stephens, J. C.; Elmes, R. B. P. The Versatility of Squaramides: From Supramolecular Chemistry to Chemical Biology. *Chem* **2019**, *5* (6), 1398−1485.

(30) Kuchar, M.; Mamat, C. Methods to Increase the Metabolic Stability of $^{18}$F-Radiotracers. *Molecules* **2015**, *20* (9), 16186−16220.

(31) Rossin, R.; Verkerk, P. R.; van den Bosch, S. M.; Vulders, R. C.; Verel, I.; Lub, J.; Robillard, M. S. In vivo chemistry for pretargeted tumor imaging in live mice. *Angew. Chem., Int. Ed.* **2010**, *49* (19), 3375−3378.

(32) Karver, M. R.; Weissleder, R.; Hilderbrand, S. A. Synthesis and Evaluation of a Series of 1,2,4,5-Tetrazines for Bioorthogonal Conjugation. *Bioconjugate Chem.* **2011**, *22* (11), 2263−2270.

(33) Wu, K.; Yee, N. A.; Srinivasan, S.; Mahmoodi, A.; Zakharian, M.; Mejia Oneto, J. M.; Royzen, M. Click activated protodrugs against cancer increase the therapeutic potential of chemotherapy through local capture and activation. *Chem. Sci.* **2021**, *12* (4), 1259−1271.

(34) Trials, C. Phase 1/2a Study of SQ3370 in Patients with Advanced Solid Tumors. https://clinicaltrials.gov/ct2/show/NCT04106492 (accessed 11 May).

(35) Andrews, U. H.; Baldwin, J. E.; Grayston, M. W. On the thermal isomerization of trans-cyclooctene to cis-cyclooctene. *J. Org. Chem.* **1982**, *47* (2), 287−292.

(36) Liu, B.; Thayumanavan, S. Substituent Effects on the pH Sensitivity of Acetals and Ketals and Their Correlation with Encapsulation Stability in Polymeric Nanogels. *J. Am. Chem. Soc.* **2017**, *139* (6), 2306−2317.

(37) Wang, M.; Vannam, R.; Lambert, W. D.; Xie, Y.; Wang, H.; Giglio, B.; Ma, X.; Wu, Z.; Fox, J.; Li, Z. Hydrophilic $^{18}$F-labeled trans-5-oxocene (oxoTCO) for efficient construction of PET agents with improved tumor-to-background ratios in neurotensin receptor (NTR) imaging. *Chem. Commun.* **2019**, *55* (17), 2485−2488.

(38) Miranda, A.; Bertoglio, D.; Glorie, D.; Stroobants, S.; Staelens, S.; Verhaeghe, J. Validation of a spatially variant resolution model for small animal brain PET studies. *Biomed Phys. Eng. Express* **2020**, *6* (4), 045001.